Discover Oncology

Analysis

Single-cell and bulk transcriptome sequencing identifies circadian rhythm disruption and cluster-specific clinical insights in colorectal tumorigenesis

Chen Liu[1] · Jingyang Liu[1] · Jing Shao[1] · Xiaoman Zhao[1] · Lin Xie[1] · Mengyao Shang[1] · Ying Li[1] · Weiming Li[2]

Received: 14 December 2024 / Accepted: 28 April 2025
Published online: 08 May 2025

Abstract

Background Colorectal cancer (CRC) is one of the most common malignant tumors in the digestive system worldwide, with its mortality ranking second among all cancers. Studies have indicated that disruptions in circadian rhythm (CR) are associated with the occurrence of various cancers; however, the relationship between CR and CRC requires further evidence, and research on the application of CR in CRC is still limited.

Methods In this study, we employed both bulk and single-cell RNA sequencing to explore the dysregulation of CR in patients with CRC. By constructing a CR subtype classifier, we conducted an in-depth analysis of the prognostic significance, the status of the tumor microenvironment, and response to immune checkpoint blockade (ICB) therapy between different CR clusters. Furthermore, we developed a CR scoring system (CRS) using machine learning to predict overall survival and identified several genes as potential targets affecting CRC prognosis.

Results Our findings revealed significant alterations in CR genes and status between CRC and normal tissues using bulk and single-cell transcriptome sequencing. Patients with CRC could be categorized into two distinct CR clusters (CR cluster 1 and 2). The prognosis of CR cluster 2, with higher epithelial-mesenchymal transition (EMT) and angiogenesis scores, was significantly worser than that of CR cluster 1. These clusters exhibited distinct levels of tumor-infiltrating lymphocytes. CR cluster 2 with a notably higher proportion of patients with microsatellite-instability-high (MSI-H), potentially benefit from ICB therapy. The proportion of patients belonging to consensus molecular subtype 4 (CMS4) in CR cluster 2 was also notably higher than in CR cluster 1. Additionally, the CRS combined with tumor stage demonstrated superior overall survival prediction efficacy compared to traditional tumor stage. We revealed a potential link between model genes (*LSAMP*, *MS4A2*, *NAV3*, *RAB3B*, *SIX4*) and the disruption of CR and patient prognosis.

Conclusion This study not only provide new insights into the assessment of CR status in CRC patients but also develop a prognosis model based on CR-related genes, offering a new tool for personalized risk assessment in CRC.

Keywords Colorectal cancer · Circadian rhythm · Immune checkpoint blockade therapy · Single-cell RNA sequencing · Prognostic model

Supplementary Information The online version contains supplementary material available at https://doi.org/10.1007/s12672-025-02521-3.

✉ Weiming Li, Liweiming1980@163.com | [1]Department of Gastroenterology, The Second Affiliated Hospital of Harbin Medical University, Harbin 150086, Heilongjiang Province, China. [2]Department of Orthopaedics, The First Affiliated Hospital of Harbin Medical University, Harbin 150001, Heilongjiang Province, China.

Abbreviations

CRC	Colorectal cancer
CR	Circadian rhythm
ICB	Immune checkpoint blockade
EMT	Epithelial-mesenchymal transition
MSI-H	Microsatellite instability-high
TILs	Tumor-infiltrating lymphocytes
CMS	Consensus molecular subtypes
DEGs	Differentially expressed genes
TCGA	The Cancer Genome Atlas
OS	Overall survival
GO	Gene Ontology
WGCNA	Weighted Gene Co-Expression Network Analysis
LASSO	Least absolute shrinkage and selection operator
ROC	Receiver operating characteristic curve
IFN-γ	Interferon gamma
COX-IS	COX-2-associated inflammatory signature
TIS	T cell inflamed score
PCA	Principal component analysis
CRRG	CR clusters-related genes
CRD	Circadian rhythm disruption

1 Introduction

Colorectal cancer (CRC) is one of the most common malignant tumor of the digestive system and ranks second in cancer-related mortality [1, 2]. Current therapeutic approaches for CRC include surgical resection [3], chemotherapy [4], radiotherapy [5], targeted therapy [6], and immunotherapy [7]. Despite the dramatic therapeutic power of these strategies, some advanced patients remain unresponsive to these treatments. Therefore, there is an urgent need to identify new mechanisms and therapeutic targets that influence the occurrence and progression of CRC.

Circadian rhythm (CR) is an internal timekeeping system that synchronizes with the 24-h cycle of day and night [8]. The molecular basis of CR arises from the coordinated expression of clock genes. The core clock genes identified in mammals include *Clock*, *Bmal1*, *Per1*, *Per2*, *Per3*, *Cry1*, *Cry2*, etc. [9], which further regulate clock-controlled genes and participate in various physiological processes such as metabolism, sleep, immunity, neural activity, and endocrine functions.

Increasing evidence suggests that circadian rhythm disruption (CRD) is closely associated with a higher incidence of tumors and can promote cancer progression [10, 11]. CRD can significantly affect the transition of the cell cycle from G0-G1 to G1-S phase, regulate tumor cells proliferation [12, 13], enhance the stemness characteristics of tumor cells [14]. CRD can also promote tumor metastasis [15]. Recent studies have shown that, at the initial stage of tumor metastasis, clock genes (such as *BMAL1*, *PER2*, and *CLOCK*) can inhibit epithelial-mesenchymal transition (EMT) by regulating *TGF-β*. Meanwhile, in the pre-metastatic environment, *BMAL1* can promote the transcription of *RAB27A* to drive CRC metastasis [13]. CRD also affect tumor metabolism. Studies have shown that sleep deficiency disrupts the rhythm of *ACSL1*, activates fatty acid oxidation through the conversion of palmitoyl to palmitoyl-coenzyme A, and promotes lung tumor growth [14].

The impact of CR on the tumor microenvironment (TME) is also important. Chronic CRD activates tumor fibroblasts, thereby increasing the proportion of tumor stem cells in tumors and promoting the dissemination of tumors from the primary site [13]. In *Bmal1*-/- mice, downregulation of plasminogen activator inhibitor-1 leads to an increase in plasminogen activators in the TME and the activation of plasmin, inducing the transformation of cancer-associated fibroblasts (CAFs) into myofibroblasts (myoCAFs) [16], which promotes tumor growth and metastasis. Additionally, the number of tumour-infiltrating lymphocytes (TILs) in mouse models shows circadian rhythmic changes, with the highest number at night. The expression of genes related to T cell activation, inhibition, migration, and effector functions in effector CD8 + T cells also show circadian rhythmic changes, and treatment with anti-PD-1 antibody at night significantly inhibits tumor growth [17]. CRD induces the accumulation of myeloid-derived suppressor cells (MDSCs) and dysfunctional CD8 + T cells in the lungs, accelerating the metastasis of CRC to the lungs [15]. Given the association between CR and cancer, CRC patients can benefit greatly from specific therapy based on CR (for example, cancer chronotherapy), which may

optimize traditional cancer therapies and even enhance new anti-cancer drugs [9]. Therefore, a systematic analysis of the CR status of CRC patients is significant for risk assessment and lifestyle interventions at every stage from prevention to survival in cancer treatment.

In this study, we integrated bulk and single-cell RNA sequencing to discover significant CRD during the development of CRC. Subsequently, we constructed a CR cluster classifier and found that different CR clusters have distinct prognoses and TME. These clusters are closely related to ICB treatment response indicators, including microsatellite-instability (MSI) status, T cell inflamed score (TIS), and *COX-2*-associated inflammatory signature (COX-IS). In addition, we constructed a CR scoring system (CRS) to predict the overall survival (OS) of CRC patients. The combination of CRS and tumor stage outperformed traditional tumor staging in terms of OS prediction efficacy. In summary, our research results provide new insights into the judgment of CR status in CRC patients and further provide potential intervention targets for CR-based treatment methods.

2 Materials and methods

2.1 Data source and processing

The transcriptomic and clinical data for colon adenocarcinoma cohort of The Cancer Genome Atlas (TCGA COAD cohort) were downloaded from the UCSC website. We converted the raw Counts data to log2(TPM + 1) for subsequent analyses [18]. The microarray datasets GSE21510 and GSE17536 were downloaded from the Gene Expression Omnibus database. Probes mapping to multiple genes were excluded, and when multiple probes corresponded to a single gene, their mean expression value was calculated and log2-transformed. GSE188688, containing RNA sequencing data from the kidneys of wild-type and Bmal1 knockout mice, was also downloaded and processed as above description. We used the *convert_mouse_to_human_symbols* function from the *nichenetr* R package to convert mouse gene symbols to their human counterparts [19]. The detailed information of the datasets used in this study was provided in Supplementary Fig. 1.

2.2 Differential expression genes analysis

Differentially expressed genes (DEGs) between two groups were identified using the *Limma* R package. For sequencing data, we utilized the raw Counts values, whereas normalized expression values were used for microarray data. DEGs were visualized using the *ggplot2* R package. DEGs with $|\log2(\text{fold change})| > 1.0$ and $p < 0.05$ were selected for further analysis.

2.3 Calculation of CRD score

To assess the degree of CRD in each sample, the CRD score was calculated based on CR associated genes using the *CRDscore* R package [20]. The bulk sequencing and microarray data were processed according to the package manual.

2.4 Assessment of CR status in single-cell transcriptomics

Single-cell transcriptomic datasets were obtained from Supplementary Data 3 of a previously published study [21]. Dimensionality reduction and clustering were performed using *Seurat V4.0* [22]. To retain high-quality cells, we filtered out cells with fewer than 200 detected genes or with mitochondrial gene content exceeding 20%. Subsequently, genes expressed in fewer than 3 cells were removed to ensure robust downstream analysis. Dimensionality reduction was performed using 20 principal components (PCs) based on principal component analysis (PCA), which effectively reduced the data dimensionality while preserving biologically relevant information. Batch effects were mitigated using the Harmony algorithm to integrate datasets across different conditions [23]. For cell clustering, the Louvain algorithm was employed due to its superior performance in handling large-scale datasets. A resolution parameter of 0.8 was selected for clustering, which was determined through iterative optimization to achieve an optimal balance between cluster granularity and biological accuracy. Cell subpopulations were annotated based on marker genes provided by the original authors, resulting in the classification of cells into T, B, stromal, epithelial, and myeloid cells. We retrieved CR-related gene sets by searching the MSigDB database (2023.2.Hs) with the keyword "circadian rhythm," ultimately identifying the GOBP-CIRCADIAN-RHYTHM gene set (Supplementary Data 1) [24]. Based on this gene set, we utilized the *irGSEA* R package to score and visualize the CR gene sets within the single-cell transcriptomic data [25].

2.5 Unsupervised clustering

Unsupervised clustering was performed using *ConsensusClusterPlus*, a tool widely used in bioinformatics and biomedical research [26]. We conducted unsupervised clustering on bulk transcriptome expression matrices using a manually curated set of 48 CR genes (Supplementary Data 2) [27]. The clustering algorithm was configured with the following parameters: 80% item resampling (*pItem*), 100% gene resampling (*pFeature*), 1000 iterations (*reps*), and K-means clustering with Euclidean distance (*clusterAlg*).

2.6 Functional enrichment analysis

Gene Ontology (GO) analysis of differentially expressed genes (DEGs) was conducted using the *clusterProfiler* R package [28]. Adjusted P-value less than 0.05 was considered statistically significant. The results of the enrichment analysis were visualized using the *ggplot2* R package.

2.7 Kaplan–Meier analysis

Patients' survival times were converted to months, and samples with survival times less than one month were excluded. The *survminer* R package was used to visualize survival status across different groups and generate Kaplan–Meier (KM) plots. For continuous gene expression values, the optimal cutoff was determined using the *survminer* package, after which patients were divided into high and low expression groups. The log-rank test was used to assess the statistical significance of survival differences.

2.8 Weighted gene co-expression network analysis

Weighted gene co-expression network analysis (WGCNA) was utilized to identify gene modules most associated with CR clusters [29]. The *WGCNA* R package was used with default parameters. Specifically, in the TCGA COAD cohort, CR cluster 1 and cluster 2 were used as input traits, with the top 50% of genes by variance used as input genes. Pearson correlation was used to analyze the relationships between module genes and traits.

2.9 Assessment of consensus molecular subtype (CMS) classification

The CMS of CRC include CMS1 (MSI Immune), CMS2 (Canonical), CMS3 (Metabolic), and CMS4 (Mesenchymal) [30]. CMS1 is characterized by microsatellite-instability-high (MSI-H) and high immune cell activation, making patients more responsive to immunotherapy. CMS2 typically features *Wnt* and *Myc* pathway activation, lower immunogenicity, and better overall prognosis. CMS3 is marked by significant metabolic abnormalities, including glucose, lipid, and nucleotide metabolism, and lower tumor immunogenicity. CMS4 is associated with *TGF-β* activation, stromal invasion, and angiogenesis, correlating with poorer OS and relapse-free survival (RFS). In this study, CMS classification for the TCGA COAD and GSE17536 cohorts was determined using the *CMScaller* R package based on transcriptomic data (Supplementary Data 3) [31].

2.10 Estimation of tumor-infiltrating lymphocytes

The R package *immunedeconv* was used to estimate the content of tumor-infiltrating lymphocytes (TILs) [32], which includes six immune estimation algorithms, such as ABIS, CIBERSORT, CIBERSORT-ABS, EPIC, ESTIMATE, and xCell.

2.11 Collection of ICB therapy-related biomarkers

The T cell inflamed score (TIS), which positively correlates with ICB therapy response, was calculated based on 18 *IFN-γ*-responsive genes and their corresponding weights (Supplementary Data 4) [33]. The *COX-2*-associated inflammatory signature (COX-IS), which negatively correlates with ICB therapy response, was derived from previous studies using pro-tumor and anti-tumor inflammatory factors (Supplementary Data 4) [34]. The MSI status of TCGA COAD

patients was obtained from supplementary data of previous research, identifying 72 patients as MSI-H and 355 as MSI-L/MSS (Supplementary Data 4) [35].

2.12 Construction and validation of CRS

The TCGA COAD cohort served as the training set, with the GSE17536 cohort used for validation. Candidate genes identified through WGCNA and DEGs analysis were subjected to univariate Cox regression analysis. Genes with a p-value < 0.2 were included in the least absolute shrinkage and selection operator (LASSO) regression [36] Using tenfold cross-validation, five robust genes were identified. These five genes were then included in multivariate Cox regression analysis to determine the regression coefficients for each gene.

$$\mathrm{CRS} = \mathit{NAV3} * 1.36 + \mathit{SIX4} * 0.74 - \mathit{MS4A2} * 0.4 - \mathit{RAB3B} * 0.67 - \mathit{LSAMP} * 0.5.$$

Based on the optimal cutoff value determined by the *survminer* package, samples were divided into high-score and low-score groups (Supplementary Data 5). Prognostic differences between groups were analyzed using the log-rank test. KM plots were generated using the survival and *survminer* packages, and receiver operating characteristic curve (ROC) was generated using the *timeROC* package.

2.13 Construction of nomogram

Based on the results of multivariate Cox regression analysis, a prognostic nomogram was constructed, integrating patient age, tumor stage, and CRS in the TCGA COAD cohort (excluding patients with incomplete data). The nomogram was visualized using the *rms* R package.

2.14 Statistical analysis

Statistical analyses were conducted using R software (version 4.0). The Spearman test was used to evaluate the significance of correlations between two continuous variables. Data visualization was performed using *ggplot2*. In most cases, the Wilcoxon rank-sum test (non-parametric) was used to analyze differences in continuous variables between two groups. * indicates $p < 0.05$, ** indicates p-value < 0.01, *** indicates $p < 0.001$, and **** indicates $p < 0.0001$.

3 Results

3.1 CRD is pervasive in CRC development

To investigate the role of CR in CRC development, we compared CR-related gene expression between CRC and normal tissues using the TCGA COAD and GSE21510 cohorts (Fig. 1A). The results demonstrated that many CR-related genes were altered in CRC development. We further examined the expression of several circadian core genes (Fig. 1B), and found that in CRC tissues *ARNTL*, *CRY2*, *PER1*, and *PER3* were predominantly downregulated, while *CLOCK* and *CRY1* were upregulated. Notably, *PER2* did not show significant differences between tumor and normal tissues in either dataset. Previous studies have demonstrated that the CRD score can comprehensively assess CRD during tumorigenesis based on transcriptomic data [20]. Our analysis revealed that the CRD score was significantly elevated in CRC tissues compared to normal tissues (Fig. 1C). These bulk transcriptomics results suggest significant CRD during CRC development.

We then used single-cell RNA sequencing data to further analyze CR status across different cell subtypes. Using previously identified marker genes, we annotated cells into five subtypes: T, B, stromal, epithelial, and myeloid cells (Supplementary Fig. 2, Fig. 1D) [21]. Among all cell types, the GOBP-CIRCADIAN-RHYTHM pathway exhibited highest score in stromal cells and relatively lower score in epithelial cells, as determined by UCell algorithms (Fig. 1E). Notably, GOBP-CIRCADIAN-RHYTHM scores were lower in epithelial cells from tumor tissues compared to normal tissues (Fig. 1E). Additionally, other algorithms such as AUCell, JASMINE, singscore, ssgsea, and viper also confirmed that CR scores were significantly reduced in tumor epithelial cells (Fig. 1F, Supplementary Data 1). These results suggested a disruption of the CR in colorectal cancer epithelial cells.

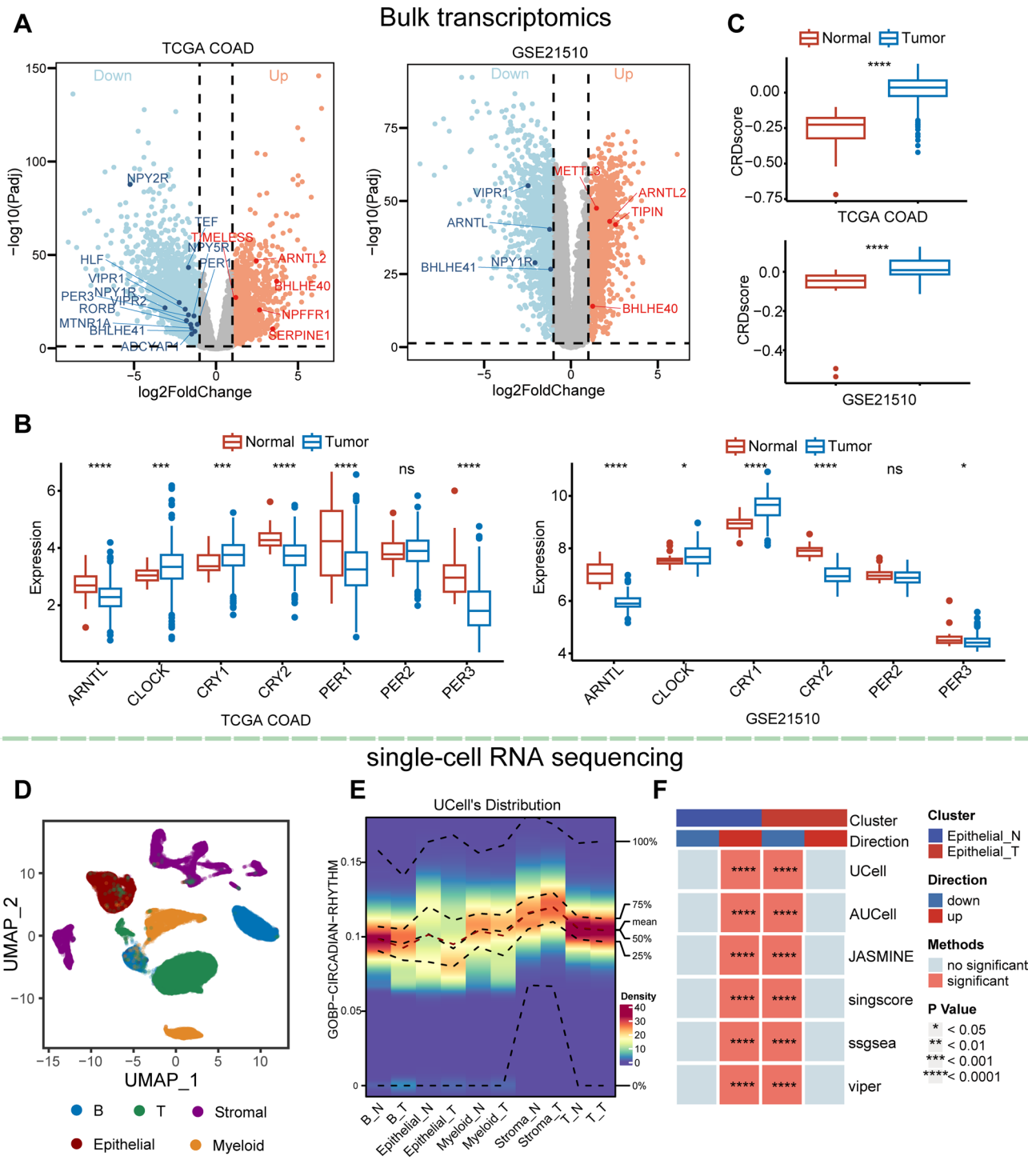

Fig. 1 Exploration of CR status in CRC using bulk and single-cell RNA sequencing. **A** Volcano plots showing differential expression analysis results between tumor and normal tissues in the TCGA COAD and GSE21510 cohorts (p.adj < 0.05, |Log2FC|> = 1). Circadian rhythm-related genes are highlighted, with red dots representing upregulated genes and blue dots representing downregulated genes. **B** Expression of seven representative core circadian genes in normal and tumor samples. The GSE21510 cohort did not include the *PER1* gene, so only six representative core circadian genes are shown. **C** CRD score expression in normal and tumor samples. **D** UMAP plot displaying cell annotations from single-cell RNA sequencing data, including B, T, stromal, epithelial, and myeloid cells. **E** Density heatmap of GOBP-CIRCADIAN-RHYTHM geneset scores across different cell subtypes using the UCell method. N represents normal tissue, and T represents tumor tissue. Analysis was performed using the *irGSEA* R package. **F** Differential expression analysis of the GOBP-CIRCADIAN-RHYTHM geneset across CR clusters using UCell, AUCell, JASMINE, singscore, ssGSEA, and viper algorithms. "Direction up" indicates upregulation, and "Direction down" indicates downregulation. Analysis was performed using the *irGSEA* R package. Wilcoxon rank-sum test (non-parametric) was used to analyze continuous variable differences between groups. * indicates p < 0.05, ** indicates p < 0.01, *** indicates p < 0.001, **** indicates p < 0.0001

3.2 CR clusters are effective in distinguishing prognostic outcomes in CRC patients

Given the widespread use of molecular subtyping in clinical practice, we manually collected 48 CR-related genes from the literature and performed unsupervised clustering on CRC patients in the TCGA COAD cohort based on these genes. We tested 2 to 9 clusters and found that the clustering was most stable when patients were divided into two groups, as indicated by the CDF plot (Fig. 2A). Therefore, we defined the two clusters as CR cluster 1 and CR cluster 2 (Supplementary Data 2). Principal component analysis (PCA) showed distinct gene expression patterns between the CR clusters (Fig. 2B). Survival analysis revealed that patients in CR cluster 1 had significantly better OS than those in cluster 2 (Fig. 2C, Log-rank $p = 0.018$). There were 95 upregulated and 684 downregulated genes in cluster 1 compared to cluster 2 (Fig. 2D, Supplementary Data 6). Subsequently, we observed that CR cluster 1 and CR cluster 2 exhibited distinct biological characteristics (Fig. 2E). CR cluster 1 was predominantly enriched in pathways related to cytoplasmic ribosomes, mitochondrial matrix, and aerobic respiration, suggesting a strong association with ribosome and mitochondrial functions, which may influence protein synthesis and energy metabolism. In contrast, CR cluster 2 was closely linked to collagen, extracellular matrix (ECM) structure, and function. These markedly different biological features between the two CR clusters may underlie their significantly divergent prognostic outcomes. We also validated these findings in the GSE17536 cohort, where the same 48 circadian genes were able to stratify patients into two distinct clusters with different gene expression patterns (Fig. 2F, Supplementary Data 2). Patients in cluster 1 had significantly better OS compared to those in cluster 2 (Fig. 2G, Log-rank $p = 0.02$). Subsequently, we observed that most CR genes were expressed at significantly lower levels in CR cluster 1 than in cluster 2 (Fig. 2H). Core clock genes such as *ARNTL*, *CLOCK*, *CRY1*, *CRY2*, *PER1*, *PER2*, and *PER3* were significantly elevated in cluster 2, indicating distinct circadian states between the two clusters (Fig. 2I).

3.3 CR clusters reflect distinct TME states

To characterize the functional differences between CR clusters, we compared the expression of previously identified biological processes between the CR clusters [37]. Compared to CR cluster 1, angiogenesis and EMT processes were significantly elevated in CR cluster 2 (Fig. 3A), suggesting a higher likelihood of metastasis in these patients. Furthermore, immune-related events such as CD8 T effector function, Pan-F-TBRS, and immune checkpoints were significantly upregulated in CR cluster 2 (Fig. 3A), indicating distinct immune states between the two clusters. Representative immune checkpoint genes also showed differential expression between CR clusters (Fig. 3C). We then applied six widely used deconvolution algorithms to assess the TILs content across the CR clusters. Overall, TILs content significantly varied between the CR clusters (Fig. 3B). Specifically, CAF and T cell dysfunction scores were higher in CR cluster 2, while M2 macrophage and MDSC scores were lower compared to CR cluster 1 (Fig. 3D). Given the close relationship between the TILs and ICB therapy response, we examined two published ICB efficacy-related markers between the CR clusters. TIS, an indicator of ICB response, was elevated in CR cluster 2, whereas COX IS, a marker of ICB resistance, was reduced (Fig. 3E). Additionally, the proportion of MSI-H patients was significantly higher in CR cluster 2 compared to MSI-L&MSS (Fig. 3F, $p = 0.00082$). These results suggest that patients in CR cluster 2 may be more responsive to ICB treatment.

3.4 Significant differences in CMS subtypes between the two CR clusters

To identify potential CR-related genes, we conducted WGCNA using the two CR clusters as phenotypic information to identify cluster-associated hub genes (Fig. 4A). The results showed that the turquoise module was most associated with the CR clusters among all modules (Fig. 4B). We identified 196 common genes between the turquoise module genes and DEGs of CR clusters, which were defined as candidate genes (Fig. 4C, Supplementary Data 6). Unsupervised clustering of the TCGA COAD cohort using these genes still stratified patients into two groups with distinct gene expression profiles and survival outcomes, which we defined as CR clusters-related genes (CRRG) clusters (Fig. 4D, E). Sankey diagram showed that most patients in CR cluster 1 are also in CRRG cluster 1 (Fig. 4F), further confirming the robustness of CR clusters.

Next, we compared the distribution of CMS across the CR/CRRG clusters and found significant differences (Fig. 4G–I). CMS1 (MSI Immune) was primarily enriched in CR/CRRG cluster 2, while CMS2 (Canonical) was more

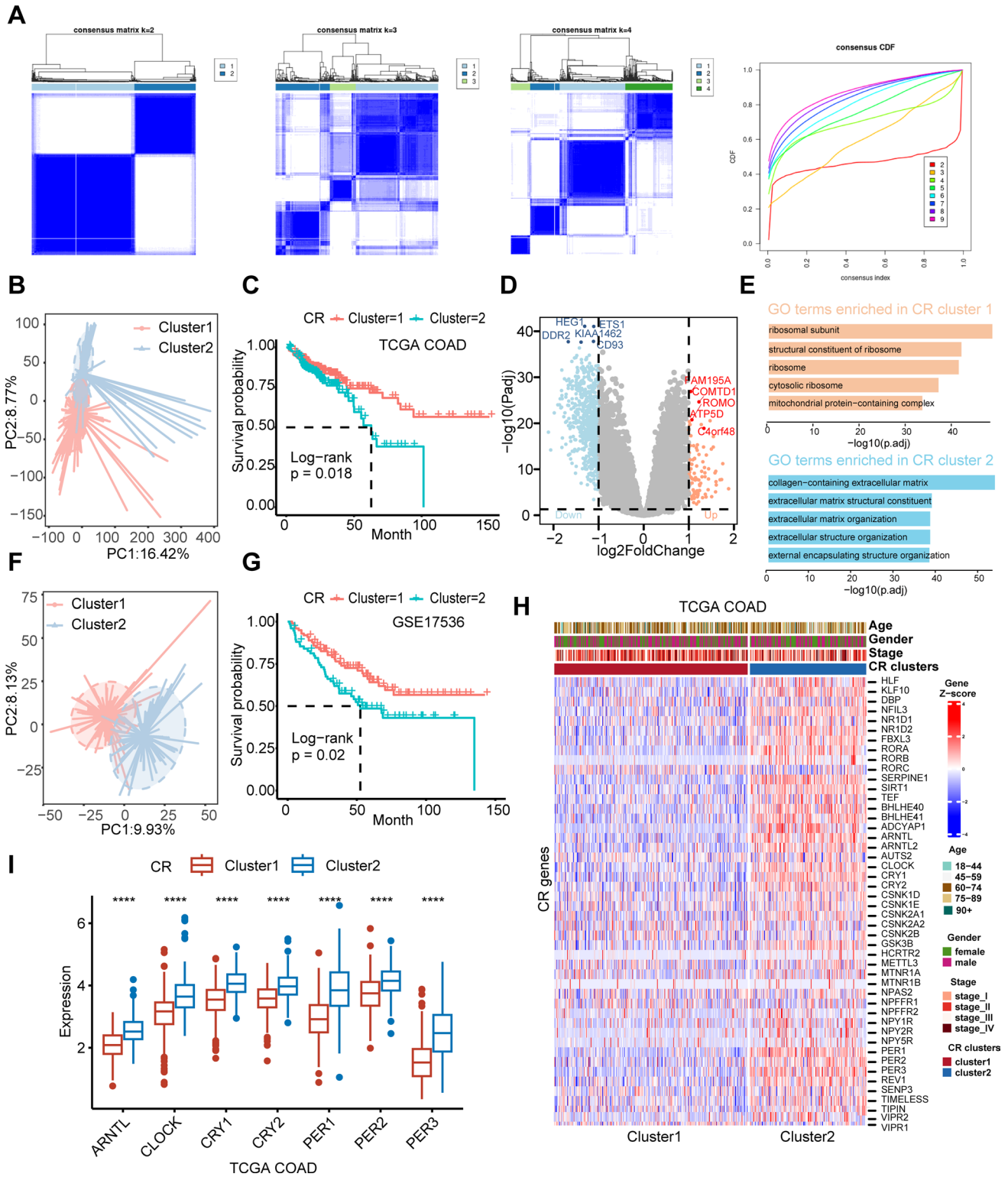

Fig. 2 Identification of CR clusters. **A** Consensus matrix generated for *k* values from 2 to 4 in the TCGA COAD cohort. Empirical cumulative distribution function (CDF) plot shows consensus distributions for each *k*. **B** PCA plot showing gene expression patterns of two CR clusters in the TCGA COAD cohort. **C** KM curves illustrating survival outcomes of two CR subtypes in the TCGA COAD cohort. **D** Volcano plot of DEGs between the two CR clusters, with the top five upregulated and downregulated genes highlighted. **E** Bar chart of GO enrichment analysis shows the top 5 significantly enriched GO terms in the two CR clusters. **F** PCA plot showing gene expression patterns of two CR clusters in the GSE17536 cohort. **G** KM plots illustrating OS of two CR clusters in the GSE17536 cohort. **H** Distribution of 48 CR-related genes between CR clusters in the TCGA COAD cohort. **I** Expression of seven representative core circadian genes between CR clusters in the TCGA COAD cohort

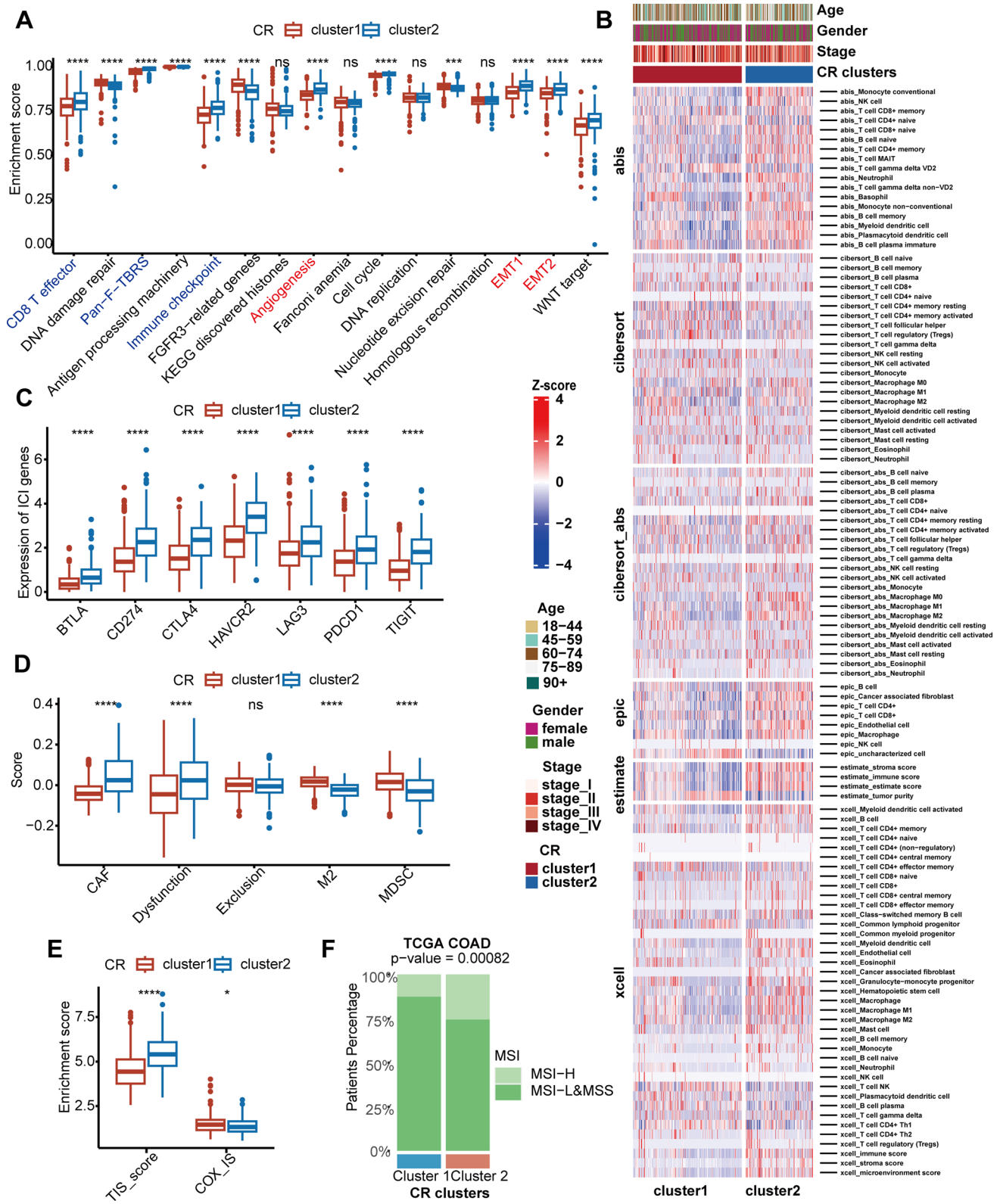

Fig. 3 Exploration of biological processes associated with CR clusters. **A** Enrichment scores for cancer-related biological processes of CR clusters. F-TBRS: pan-tissue fibroblast *TGF-β* response genes, EMT: epithelial-mesenchymal transition markers. Enrichment scores were calculated using *ssGSEA*. **B** Heatmap showing TILs content across CR clusters. ABIS, CIBERSORT, CIBERSORT-ABS, EPIC, ESTIMATE, and xCell are six widely used immune estimation algorithms. **C** Expression of common immune checkpoint genes across CR clusters. **D** Differences in CAF, Dysfunction, Exclusion, M2, and MDSC scores between CR clusters. Data were downloaded from the TIDE website. CAF: cancer-associated fibroblasts, Dysfunction: T cell dysfunction, Exclusion: T cell exclusion, M2: M2 macrophages, MDSC: myeloid-derived suppressor cells. **E** TIS and COX IS scores across CR clusters. **F** Distribution of MSI-H and MSI-L/MSS patients across CR clusters. Statistical testing was performed using Pearson's Chi-squared test

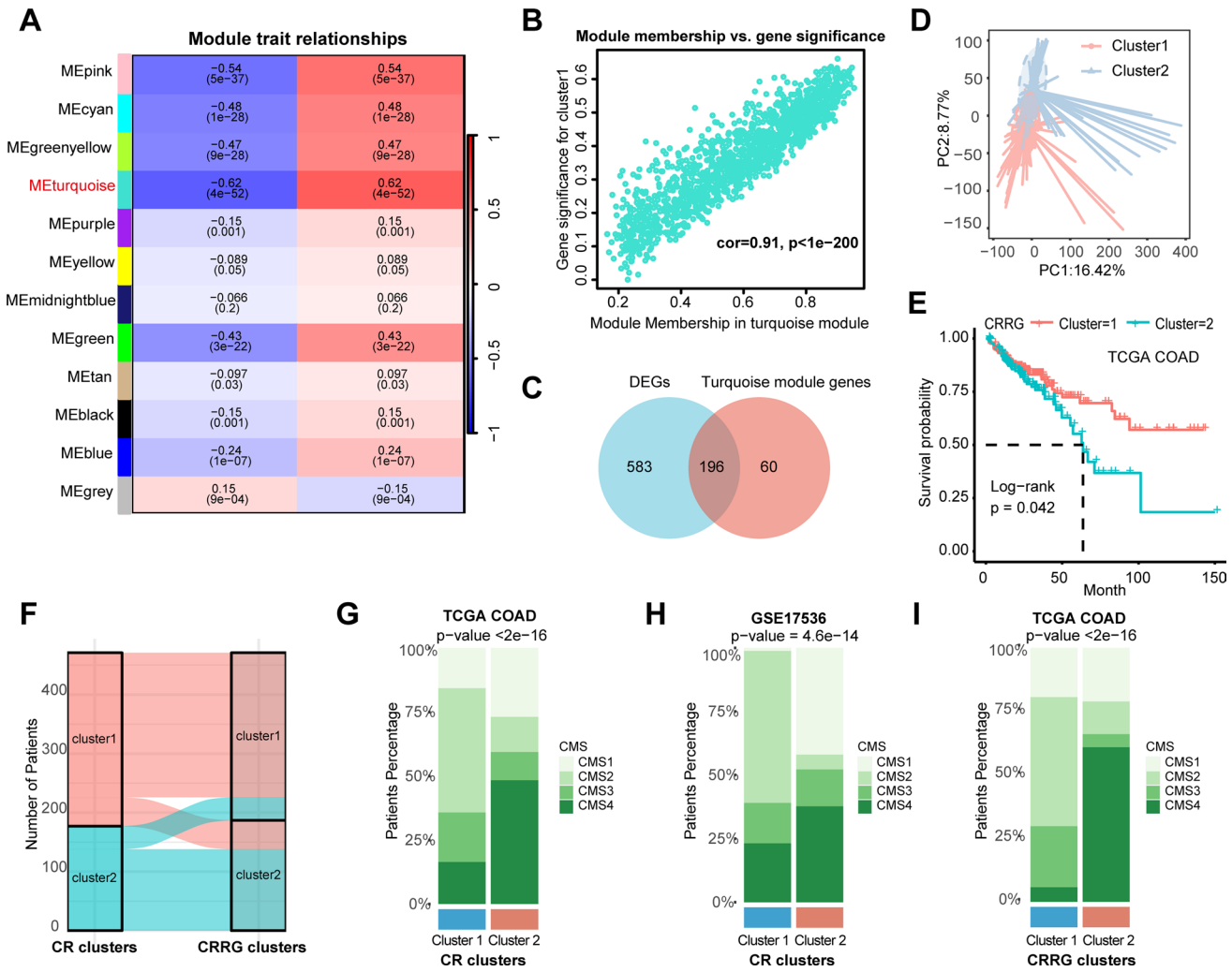

Fig. 4 Validation of CR clusters. **A** Correlation of module eigen genes with CR clusters in WGCNA analysis. Each row includes the corresponding correlation values and p-values, with red and blue indicating positive and negative correlations, respectively. **B** Detail correlation between module membership and gene significance of the turquoise module. **C** Common genes between DEGs of CR clusters and turquoise module genes. **D** PCA plot showing gene expression patterns of CRRG clusters in the TCGA COAD cohort. **E** KM plot illustrating OS of CRRG clusters in the TCGA COAD cohort. **F** Sankey plot showing the relationship between CR clusters and CRRG clusters in the TCGA COAD cohort. **G**–**I** The distribution of CMS1-4 in CR clusters (**G**: TCGA COAD; **H**: GSE17536) and CRRG clusters (**I**: TCGA COAD). Statistical testing was performed using Pearson's Chi-squared test

prevalent in CR/CRRG cluster 1. Notably, CMS4 was mainly distributed in CR/CRRG cluster 2. Compared to CMS1-3 clusters, CMS4 is characterized by a high stromal content and is recognized as a poorer prognostic subtype in CRC, which may partly explain the worse prognosis of patients in CR/CRRG cluster 2.

3.5 CRS combined with tumor stage outperforms stage alone in predicting overall survival of CRC patients

We used candidate genes identified from WGCNA and DEG analyses to construct a prognostic model based on LASSO and multivariate Cox regression analyses, which we termed the CR-related score (CRS). These figures illustrate the feature selection process using LASSO (Fig. 5A, B). Finally, we identified five robust genes and their corresponding regression coefficients. According to the methods described, patients were divided into high and low CRS groups, with the high CRS group showing significantly worse OS compared to the low CRS group (Fig. 5C: training cohort; Fig. 5D: validation cohort). The predictive power of CRS combined with tumor stage for 1-, 3-, and 5-year OS was 0.85, 0.84, and 0.79, respectively, significantly better than that of tumor stage alone (0.72, 0.72, 0.66) (Fig. 5E, F: TCGA COAD). This result was also observed in the GSE17536 cohort (Fig. 5G, H). Additionally, CRS was significantly elevated in patients with tumor metastasis and

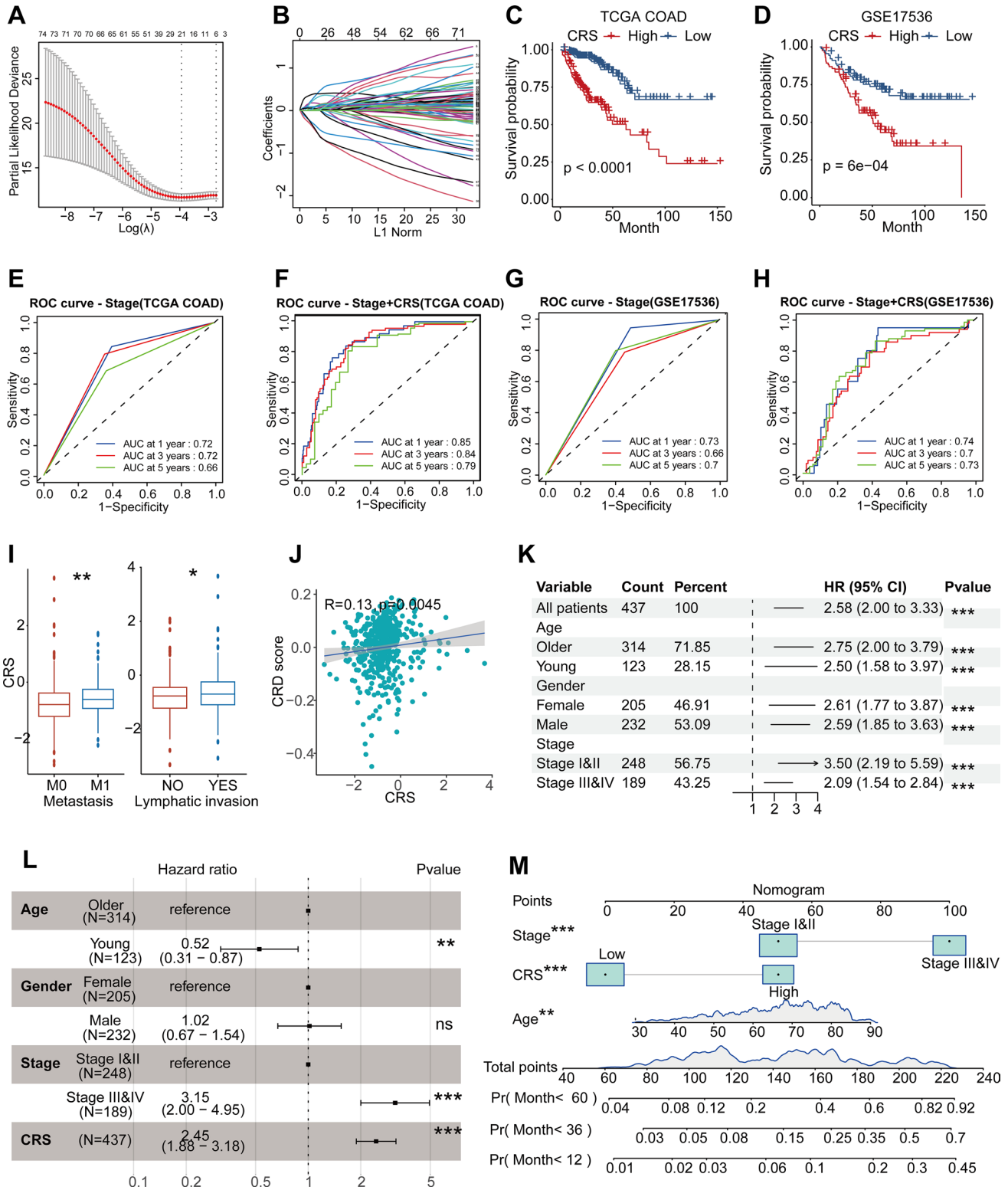

Fig. 5 Development of the CRS prognostic model. **A**, **B** LASSO regression analysis for selecting variables for the prognostic model. **C**, **D** KM plots showing survival differences between high and low CRS groups. **E**–**H** ROC plots showing the predictive performance of tumor stage and tumor stage + CRS for OS in cancer patients (**E**, **F**: TCGA COAD cohort; **G**, **H**: GSE17536 cohort). **I**–**M** Data from the TCGA COAD cohort. **I** CRS levels in metastatic patients (M1) versus non-metastatic patients (M0), lymph node invasion (YES) versus no lymph node invasion (NO). **J** Spearman correlation analysis between CRS and CRD score. **K** Univariate Cox regression analysis of CRS in different clinical subgroups. **L** Multivariate Cox regression analysis including Age, Gender, Stage, and CRS. **M** Nomogram constructed using Stage, CRS, and Age for predicting 1-, 3-, and 5-year OS in cancer patients. ** indicates $p < 0.01$, *** indicates $p < 0.001$

lymph node invasion compared to those without these conditions (Fig. 5I). CRS was also significantly positively correlated with the previously proposed CRD score (Fig. 5J). Subgroup analysis indicated that CRS was a significant risk factor across different tumor subgroups (Older, Young, Female, Male, Stage I&II, and Stage III&IV) (Fig. 5K). Multivariate Cox regression analysis incorporating age, gender, and tumor stage confirmed that CRS remained a risk factor after adjusting for these variables (Fig. 5L). Finally, a nomogram was constructed using variables that were meaningful in the multivariate Cox regression analysis (tumor stage, CRS, and age) to predict 1-, 3-, and 5-year overall survival in CRC patients (Fig. 5M).

Furthermore, we manually collected 65 mRNA-based prognostic models for CRC from the literature (Supplementary Data 7) and evaluated the prognostic performance of the CRS model compared to existing models using C-index and AUC. For each model, we calculated the C-index and AUC values for 1-year, 3-year, and 5-year overall survival in both the TCGA COAD and GSE17536 cohorts, using the average value of each index to comprehensively measure the model's prognostic performance. The results showed that the CRS achieved the highest C-index, 3-year AUC, and 5-year AUC values among all models, while the 1-year AUC ranked fourth (Fig. 6). These findings suggested that the CRS score exhibited superior efficacy in prognostic prediction.

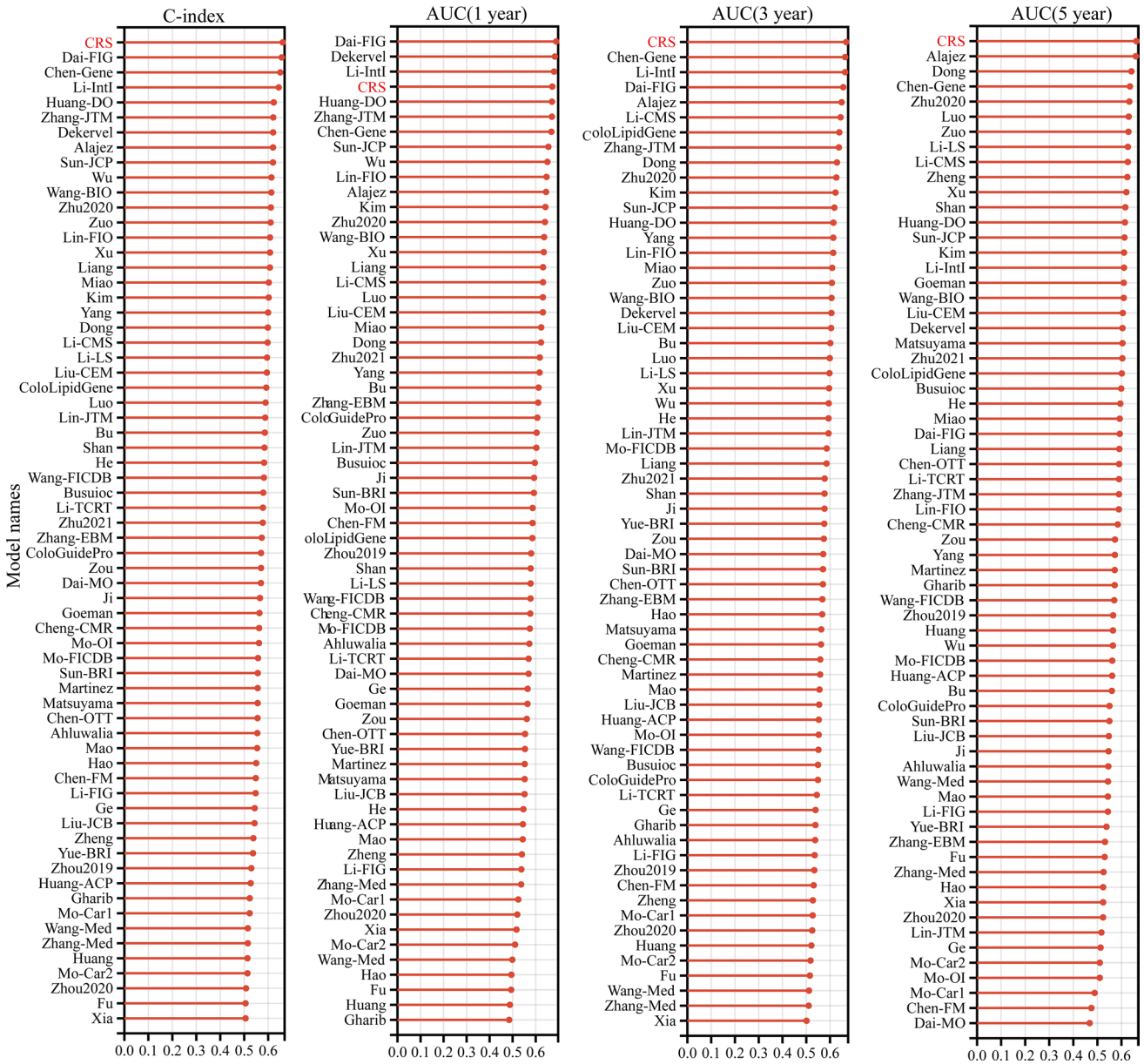

Fig. 6 Comparison of prognostic performance of CRS and other CRC models. This figure compares the prognostic performance of the CRS model with 65 other mRNA-based CRC prognostic models in terms of C-index and AUC values (AUC refers to the Area Under the ROC Curve)

3.6 Exploring the relationship between CRS model genes and circadian rhythms

In the TCGA COAD cohort, we found that the expression levels of nearly all core circadian rhythm genes were significantly positively correlated with the CRS model genes (Supplementary Fig. 3). As transcription factors, the core clock genes *CLOCK* and *BMAL1* may play an important role in driving the transcription of CRS model genes. To verify this, we used the TF-Target Finder online tool to identify potential transcription factor-target gene interactions [38]. TF-Target Finder showed that the Gene Transcription Regulation Database suggested that *LSAMP*, *NAV3*, and *SIX4* might be downstream target genes of *CLOCK* (Supplementary Data 8) [39]. Unfortunately, *BMAL1* was not included in the database. Taken together, these results suggested that core circadian rhythm genes such as *CLOCK* may regulate the transcription of genes like *LSAMP*, *NAV3*, and *SIX4*, thereby influencing their expression and CRC progression.

To explore potential drug targets for CRS model genes, we used the oncoPredict R package to predict the half-maximal inhibitory concentration (IC50) of 198 drugs in TCGA COAD patients. We then analyzed the correlation between CRS model genes and the IC50 values of these drugs. A correlation was considered significant if $p < 0.05$ and the correlation coefficient > 0.3 (Supplementary Fig. 4). For example, *MS4A2* showed a negative correlation with ABT737_1910, suggesting that patients with high *MS4A2* expression may be more sensitive to this drug. *RAB3B*, *NAV3*, *MS4A2*, and *LSAMP* were positively correlated with Acetalax_1804, indicating that patients with high expression of these genes may be less sensitive to Acetalax_1804. Subsequently, we observed that the CRS model genes (*LSAMP*, *MS4A2*, *NAV3*, *RAB3B*, and *SIX4*) were significantly negatively correlated with the CRD score (Fig. 7A–E). And the expression levels of *Ms4a2* and *Rab3b* were higher in *Baml* knockout group compared to the wild-type group (Fig. 7F), suggesting that these genes may be regulated by circadian rhythms. Moreover, KM plots indicated that patients with high expression of *LSAMP*, *MS4A2*, and *RAB3B*, as well as low expression of *NAV3* and *SIX4*, had better OS (Fig. 7G–K). Thus, these genes might serve as potential intervention targets influencing CRC prognosis.

4 Discussion

Despite growing awareness of the impact of CR regulation in cancer [13, 14, 17], systematic analysis of CR status in CRC patients holds significant potential for risk assessment and targeted lifestyle interventions across all stages of cancer management, from prevention to survival.

Single-cell RNA sequencing enables gene expression analysis at the individual cell level, offering a finer resolution compared to bulk sequencing [40–42]. In this study, we integrated two types of sequencing methods and found significant differences in CRD score, core CR genes, and CR pathway scores between CRC and normal tissues, indicating marked alterations in CR status during tumorigenesis.

CR profoundly influence metabolic states [43], for example, sleep deficiency activates fatty acid oxidation, which promotes lung tumor growth. Our study revealed that the differentially biological functions between CR clusters are predominantly enriched in categories such as cytosolic ribosome, mitochondrial matrix, and aerobic respiration (Fig. 2E). Thus, we inferred that CR status affects CRC primarily through its impact on energy metabolism and protein synthesis, which represent crucial future directions for CR research.

CR status also affects EMT and metastasis. Clock genes (*BMAL1*, *PER2*, and *CLOCK*) can inhibit EMT by regulating *TGF-β* transcription factors [13]. Disrupted CR can accelerate cancer metastasis by triggering the accumulation of myeloid-derived suppressor cells through gut microbiota [15]. In our study, we observed significant differences in the proportion of CMS4 (characterized by EMT) between CR clusters. And *ssGSEA* analysis revealed distinct EMT scores across CR clusters. These suggest that CR-based therapies may offer promising treatments for metastatic CRC [44].

Currently, the decision to administer ICB therapy in CRC patients primarily depends on MSI status [45]. MSI-H patients are recommended for ICB treatment, but this approach does not fully predict patient response to ICB therapy [46]. In this study, we found that significant differences in the proportions of MSI-H and MSI-L/MSS between CR clusters. Moreover, ICB markers (TIS, COX-IS) also vary across CR clusters. Combining MSI status and CR clusters classification to predict responses to ICB therapy is promising. Additionally, CRS demonstrates excellent predictive performance for CRC patient outcomes. Combining CRS with tumor stage significantly enhances OS prediction, with 1-, 3-, and 5-year AUC values exceeding 0.7, compared to tumor stage alone.

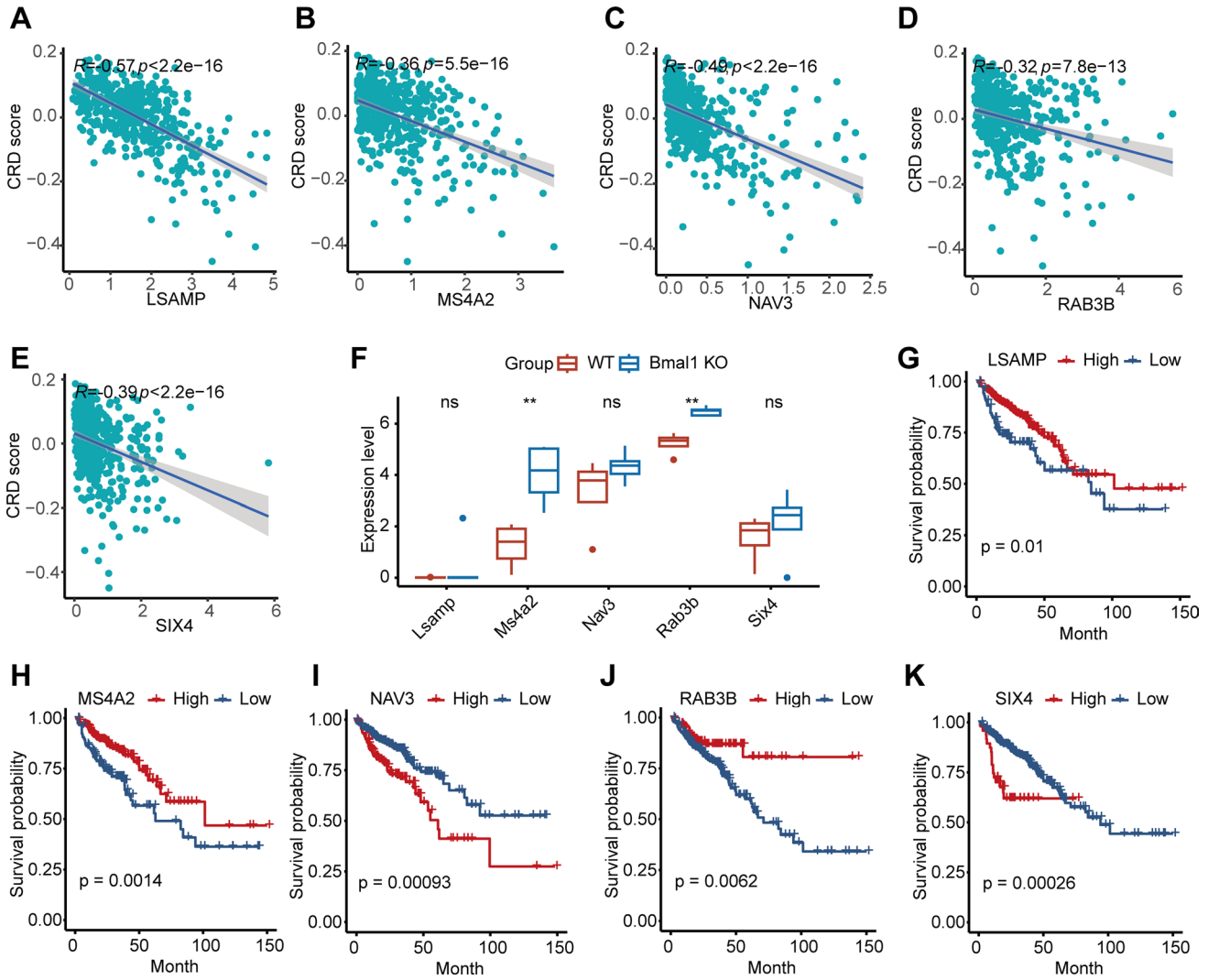

Fig. 7 Identification of potential targets for improving CRC prognosis. **A**–**E** Spearman correlation analysis between CRD score and CRS model genes (*LSAMP*, *MS4A2*, *NAV3*, *RAB3B*, and *SIX4*) in the TCGA COAD cohort. **F** Expression levels of CRS model genes in wild type and *Bmal1* knockout mouse kidney tissues (GSE188688). Statistical significance between groups was tested using t-test. *WT* wild type, *Bmal1 KO* *Bmal1* knockout. **G**–**K** Survival analysis of CRS model genes in the TCGA COAD cohort

Previous studies have shown that *LSAMP* reexpression inhibits tumor growth in preclinical osteosarcoma models [47]. Although research on *MS4A2* in tumors is limited, bioinformatics studies have identified it as a mast cell marker in CRC [48]. *SIX4* promotes hepatocellular carcinoma metastasis by upregulating *YAP1* and *c-MET*, serving as a prognostic biomarker for HCC patients [49]. *NAV3* may suppress breast cancer progression by modulating microtubule dynamics, directional migration, and inhibiting initial cell movement [50]. In a mouse xenograft model, *Rab3B* enhances DDX6 stability and promotes lung adenocarcinoma growth [51]. In CRC, RT-PCR has indicated that *NAV3* expression was significantly elevated in CRC cells, and its knockdown inhibited CRC cell proliferation [52]. *LSAMP* might enhance the sensitivity of CRC cells to CD8 + T cell-mediated cytotoxicity by inhibiting the Wnt/β-catenin signaling pathway [53]. The mRNA level of *RAB3B* was lower in tumor tissues compared to adjacent non-malignant tissues [54]. *SIX4* was highly expressed in tumor tissues, and its overexpression promoted tumor growth and angiogenesis both in vitro and in vivo [55]. Silencing *SIX4* inhibited CRC cell metastasis by suppressing AKT phosphorylation [56]. However, high-quality studies that specifically investigate the roles of these model genes in CRC and their potential relationship with CRD are still lacking.

Our study also identified CRS model genes associated with CRC prognosis, where high expression of *LSAMP*, *MS4A2*, and *RAB3B*, and low expression of *NAV3* and *SIX4*, correlated with better outcomes. Furthermore, CRS model genes were significantly negatively correlated with the CRD score; in *Baml1* knockout mouse kidney tissues, expression of *Ms4a2* and *Rab3b*

was higher than in wild-type mice. Understanding whether these genes are influenced by CRD and affect the prognosis of CRC is a critical focus for future studies.

The causality of CRD and CRC is an interesting issue. Numerous studies have shown that CRD can increase the risk of CRC. For example, research has found that CRD can disrupt the balance of the gut microbiome and the integrity of the intestinal barrier, which in turn promotes the development of CRC [57]. Additionally, CRD can overactivate the Wnt signaling pathway and enhance MYC-dependent glycolytic metabolism, thereby accelerating the progression of CRC [58]. These findings suggest that CRD may be a significant driver of CRC initiation and progression. Although CRC may indirectly cause CRD by affecting patients' physiological states (e.g., sleep quality), current evidence more strongly supports CRD as a driver of CRC.

4.1 Limitations

The results of this study are based on publicly available transcriptomic sequencing data from large cohort samples. Further validation using data from our institution will be necessary in the future. Additionally, in vivo and in vitro studies are needed to validate the relationship between core circadian genes and CRS model genes in CRC tissues. A critical area for future research is to determine whether these genes are regulated by CR and how this regulation might impact CRC prognosis.

5 Conclusion

There are significant changes in CR states during CRC development. The CR clusters represent two distinct CR states. CRS plays a crucial role in personalized assessment of CRC prognosis. *LSAMP*, *MS4A2*, *RAB3B*, *NAV3*, and *SIX4* may be potential prognostic targets regulated by CR.

Acknowledgements The authors would like to express their sincere gratitude for the support provided by the First and Second Affiliated Hospitals of Harbin Medical University for this project.

Author contributions CL conducted the experimental design, data collection, analysis, and interpretation, and drafted the initial manuscript. JYL, XMZ and LX participated in the experimental design and data collection, provided significant support in data analysis, and contributed to the writing and revision of the manuscript. JS, MYS and YL engaged in experimental procedures and data collection, offered suggestions for the improvement of experimental methods, and reviewed the initial draft of the manuscript. WML oversaw and directed the overall research, provided critical guidance on study design and data analysis, and reviewed and approved the final version of the manuscript.

Funding This work was supported by the Heilongjiang Postdoctoral Scientific Developmental Fund (Grant No. LBH-Q20044).

Data availability The datasets used and/or analysed during the current study available from the corresponding author on reasonable request.

Declarations

Ethics approval and consent to participate The data utilized in this article did not involve any ethical considerations.

Consent for publication All the authors agree for the publication.

Competing interests The authors declare no competing interests.

References

1. Sung H, Ferlay J, Siegel RL, Laversanne M, Soerjomataram I, Jemal A, Bray F. Global Cancer Statistics 2020: GLOBOCAN estimates of incidence and mortality worldwide for 36 cancers in 185 countries. CA Cancer J Clin. 2021;71:209–49.

2. Wójcik M, Juhas U, Mohammadi E, Mattisson J, Drężek-Chyła K, Rychlicka-Buniowska E, Bruhn-Olszewska B, Davies H, Chojnowska K, Olszewski P, Bieńkowski M, Jankowski M, Rostkowska O, Hellmann A, Pęksa R, Kowalski J, Zdrenka M, Kobiela J, Zegarski W, Biernat W, Szylberg Ł, Remiszewski P, Mieczkowski J, Filipowicz N, Dumanski JP. Loss of Y in regulatory T lymphocytes in the tumor microenvironment of primary colorectal cancers and liver metastases. Sci Rep. 2024;14:9458.
3. Yin TC, Su WC, Chen PJ, Chang TK, Chen YC, Li CC, Hsieh YC, Tsai HL, Huang CW, Wang JY. Oncological outcomes of robotic-assisted surgery with high dissection and selective ligation technique for sigmoid colon and rectal cancer. Front Oncol. 2020;10: 570376.
4. Glimelius B, Stintzing S, Marshall J, Yoshino T, de Gramont A. Metastatic colorectal cancer: advances in the folate-fluoropyrimidine chemotherapy backbone. Cancer Treat Rev. 2021;98: 102218.
5. Wang H, Li X, Peng R, Wang Y, Wang J. Stereotactic ablative radiotherapy for colorectal cancer liver metastasis. Semin Cancer Biol. 2021;71:21–32.
6. Singh M, Morris VK, Bandey IN, Hong DS, Kopetz S. Advancements in combining targeted therapy and immunotherapy for colorectal cancer. Trends Cancer. 2024;10:598–609.
7. Ganesh K, Stadler ZK, Cercek A, Mendelsohn RB, Shia J, Segal NH, Diaz LA Jr. Immunotherapy in colorectal cancer: rationale, challenges and potential. Nat Rev Gastroenterol Hepatol. 2019;16:361–75.
8. Bass J, Takahashi JS. Circadian integration of metabolism and energetics. Science (New York, NY). 2010;330:1349–54.
9. Zhu X, Maier G, Panda S. Learning from circadian rhythm to transform cancer prevention, prognosis, and survivorship care. Trends Cancer. 2024;10:196–207.
10. Filipski E, King VM, Li X, Granda TG, Mormont MC, Liu X, Claustrat B, Hastings MH, Lévi F. Host circadian clock as a control point in tumor progression. J Natl Cancer Inst. 2002;94:690–7.
11. Sancar A, Van Gelder RN. Clocks, cancer, and chronochemotherapy. Science (New York, NY). 2021;371. https://doi.org/10.1126/science.abb0738.
12. Canaple L, Kakizawa T, Laudet V. The days and nights of cancer cells. Cancer Res. 2003;63:7545–52.
13. Wang Y, Narasimamurthy R, Qu M, Shi N, Guo H, Xue Y, Barker N. Circadian regulation of cancer stem cells and the tumor microenvironment during metastasis. Nat Cancer. 2024;5:546–56.
14. Peng F, Lu J, Su K, Liu X, Luo H, He B, Wang C, Zhang X, An F, Lv D, Luo Y, Su Q, Jiang T, Deng Z, He B, Xu L, Guo T, Xiang J, Gu C, Wang L, Xu G, Xu Y, Li M, Kelley KW, Cui B, Liu Q. Oncogenic fatty acid oxidation senses circadian disruption in sleep-deficiency-enhanced tumorigenesis. Cell Metab. 2024;36:1598-1618.e1511.
15. Liu JL, Xu X, Rixiati Y, Wang CY, Ni HL, Chen WS, Gong HM, Zhang ZL, Li S, Shen T, Li JM. Dysfunctional circadian clock accelerates cancer metastasis by intestinal microbiota triggering accumulation of myeloid-derived suppressor cells. Cell Metab. 2024;36:1320-1334.e1329.
16. Wu J, Jing X, Du Q, Sun X, Holgersson K, Gao J, He X, Hosaka K, Zhao C, Tao W, FitzGerald GA, Yang Y, Jensen LD, Cao Y. Disruption of the clock component bmal1 in mice promotes cancer metastasis through the PAI-1-TGF-β-myoCAF-dependent mechanism. Adv Sci. 2023;10: e2301505.
17. Wang C, Zeng Q, Gül ZM, Wang S, Pick R, Cheng P, Bill R, Wu Y, Naulaerts S, Barnoud C, Hsueh PC, Moller SH, Cenerenti M, Sun M, Su Z, Jemelin S, Petrenko V, Dibner C, Hugues S, Jandus C, Li Z, Michielin O, Ho PC, Garg AD, Simonetta F, Pittet MJ, Scheiermann C. Circadian tumor infiltration and function of CD8(+) T cells dictate immunotherapy efficacy. Cell. 2024;187:2690-2702.e2617.
18. Navarro Gonzalez J, Zweig AS, Speir ML, Schmelter D, Rosenbloom KR, Raney BJ, Powell CC, Nassar LR, Maulding ND, Lee CM, Lee BT, Hinrichs AS, Fyfe AC, Fernandes JD, Diekhans M, Clawson H, Casper J, Benet-Pagès A, Barber GP, Haussler D, Kuhn RM, Haeussler M, Kent WJ. The UCSC Genome Browser database: 2021 update. Nucleic Acids Res. 2021;49(2021):D1046-d1057.
19. Browaeys R, Saelens W, Saeys Y. NicheNet: modeling intercellular communication by linking ligands to target genes. Nat Methods. 2020;17:159–62.
20. He L, Fan Y, Zhang Y, Tu T, Zhang Q, Yuan F, Cheng C. Single-cell transcriptomic analysis reveals circadian rhythm disruption associated with poor prognosis and drug-resistance in lung adenocarcinoma. J Pineal Res. 2022;73: e12803.
21. Qi J, Sun H, Zhang Y, Wang Z, Xun Z, Li Z, Ding X, Bao R, Hong L, Jia W, Fang F, Liu H, Chen L, Zhong J, Zou D, Liu L, Han L, Ginhoux F, Liu Y, Ye Y, Su B. Single-cell and spatial analysis reveal interaction of FAP(+) fibroblasts and SPP1(+) macrophages in colorectal cancer. Nat Commun. 2022;13:1742.
22. Satija R, Farrell JA, Gennert D, Schier AF, Regev A. Spatial reconstruction of single-cell gene expression data. Nat Biotechnol. 2015;33:495–502.
23. Korsunsky I, Millard N, Fan J, Slowikowski K, Zhang F, Wei K, Baglaenko Y, Brenner M, Loh PR, Raychaudhuri S. Fast, sensitive and accurate integration of single-cell data with Harmony. Nat Methods. 2019;16:1289–96.
24. Liberzon A, Subramanian A, Pinchback R, Thorvaldsdóttir H, Tamayo P, Mesirov JP. Molecular signatures database (MSigDB) 3.0. Bioinformatics (Oxford, England). 2011;27:1739–40.
25. Fan C, Chen F, Chen Y, Huang L, Wang M, Liu Y, Wang Y, Guo H, Zheng N, Liu Y, Wang H, Ma L. irGSEA: the integration of single-cell rank-based gene set enrichment analysis, Brief Bioinform. 2024;25. https://doi.org/10.1093/bib/bbae243.
26. Wilkerson MD, Hayes DN. ConsensusClusterPlus: a class discovery tool with confidence assessments and item tracking. Bioinformatics (Oxford, England). 2010;26:1572–3.
27. Liu Y, Guo S, Sun Y, Zhang C, Gan J, Ning S, Wang J. CRS: a circadian rhythm score model for predicting prognosis and treatment response in cancer patients. J Transl Med. 2023;21:185.
28. Yu G, Wang LG, Han Y, He QY. clusterProfiler: an R package for comparing biological themes among gene clusters. OMICS. 2012;16:284–7.
29. Langfelder P, Horvath S. WGCNA: an R package for weighted correlation network analysis. BMC Bioinform. 2008;9:559.
30. Guinney J, Dienstmann R, Wang X, de Reyniès A, Schlicker A, Soneson C, Marisa L, Roepman P, Nyamundanda G, Angelino P, Bot BM, Morris JS, Simon IM, Gerster S, Fessler E, De Sousa EMF, Missiaglia E, Ramay H, Barras D, Homicsko K, Maru D, Manyam GC, Broom B, Boige V, Perez-Villamil B, Laderas T, Salazar R, Gray JW, Hanahan D, Tabernero J, Bernards R, Friend SH, Laurent-Puig P, Medema JP, Sadanandam A, Wessels L, Delorenzi M, Kopetz S, Vermeulen L, Tejpar S. The consensus molecular subtypes of colorectal cancer. Nat Med. 2015;21:1350–6.
31. Eide PW, Bruun J, Lothe RA, Sveen A. CMScaller: an R package for consensus molecular subtyping of colorectal cancer pre-clinical models. Sci Rep. 2017;7:16618.

32. Sturm G, Finotello F, Petitprez F, Zhang JD, Baumbach J, Fridman WH, List M, Aneichyk T. Comprehensive evaluation of transcriptome-based cell-type quantification methods for immuno-oncology. Bioinformatics (Oxford, England). 2019;35:i436–45.
33. Ayers M, Lunceford J, Nebozhyn M, Murphy E, Loboda A, Kaufman DR, Albright A, Cheng JD, Kang SP, Shankaran V, Piha-Paul SA, Yearley J, Seiwert TY, Ribas A, McClanahan TK. IFN-γ-related mRNA profile predicts clinical response to PD-1 blockade. J Clin Investig. 2017;127:2930–40.
34. Pelly VS, Moeini A, Roelofsen LM, Bonavita E, Bell CR, Hutton C, Blanco-Gomez A, Banyard A, Bromley CP, Flanagan E, Chiang SC, Jørgensen C, Schumacher TN, Thommen DS, Zelenay S. Anti-inflammatory drugs remodel the tumor immune environment to enhance immune checkpoint blockade efficacy. Cancer Discov. 2021;11:2602–19.
35. Jia P, Yang X, Guo L, Liu B, Lin J, Liang H, Sun J, Zhang C, Ye K. MSIsensor-pro: fast accurate, and matched-normal-sample-free detection of microsatellite instability. Genomics Proteom Bioinform. 2020;18:65–71.
36. Friedman J, Hastie T, Tibshirani R. Regularization paths for generalized linear models via coordinate descent. J Stat Softw. 2010;33:1–22.
37. Mariathasan S, Turley SJ, Nickles D, Castiglioni A, Yuen K, Wang Y, Kadel EE III, Koeppen H, Astarita JL, Cubas R, Jhunjhunwala S, Banchereau R, Yang Y, Guan Y, Chalouni C, Ziai J, Şenbabaoğlu Y, Santoro S, Sheinson D, Hung J, Giltnane JM, Pierce AA, Mesh K, Lianoglou S, Riegler J, Carano RAD, Eriksson P, Höglund M, Somarriba L, Halligan DL, van der Heijden MS, Loriot Y, Rosenberg JE, Fong L, Mellman I, Chen DS, Green M, Derleth C, Fine GD, Hegde PS, Bourgon R, Powles T. TGFβ attenuates tumour response to PD-L1 blockade by contributing to exclusion of T cells. Nature. 2018;554:544–8.
38. Wang J. TFTF: an R-based integrative tool for decoding human transcription factor-target interactions. Biomolecules. 2024;14. https://doi.org/10.3390/biom14070749.
39. Yevshin I, Sharipov R, Kolmykov S, Kondrakhin Y, Kolpakov F. GTRD: a database on gene transcription regulation-2019 update. Nucleic Acids Res. 2019;47:D100-d105.
40. Potter SS. Single-cell RNA sequencing for the study of development, physiology and disease. Nat Rev Nephrol. 2018;14:479–92.
41. Jia Q, Chu H, Jin Z, Long H, Zhu B. High-throughput single-cell sequencing in cancer research. Signal Transduct Target Ther. 2022;7:145.
42. Li PH, Kong XY, He YZ, Liu Y, Peng X, Li ZH, Xu H, Luo H, Park J. Recent developments in application of single-cell RNA sequencing in the tumour immune microenvironment and cancer therapy. Mil Med Res. 2022;9:52.
43. Masri S, Sassone-Corsi P. The emerging link between cancer, metabolism, and circadian rhythms. Nat Med. 2018;24:1795–803.
44. Ruan W, Yuan X, Eltzschig HK. Circadian rhythm as a therapeutic target. Nat Rev Drug Discov. 2021;20:287–307.
45. Dudley JC, Lin MT, Le DT, Eshleman JR. Microsatellite instability as a biomarker for PD-1 blockade. Clin Cancer Res. 2016;22:813–20.
46. Gao Y, Bi D, Xie R, Li M, Guo J, Liu H, Guo X, Fang J, Ding T, Zhu H, Cao Y, Xing M, Zheng J, Xu Q, Xu Q, Wei Q, Qin H. Fusobacterium nucleatum enhances the efficacy of PD-L1 blockade in colorectal cancer. Signal Transduct Target Therapy. 2021;6:398.
47. Barøy T, Kresse SH, Skårn M, Stabell M, Castro R, Lauvrak S, Llombart-Bosch A, Myklebost O, Meza-Zepeda LA. Reexpression of LSAMP inhibits tumor growth in a preclinical osteosarcoma model. Mol Cancer. 2014;13:93.
48. Xie Z, Niu L, Zheng G, Du K, Dai S, Li R, Dan H, Duan L, Wu H, Ren G, Dou X, Feng F, Zhang J, Zheng J. Single-cell analysis unveils activation of mast cells in colorectal cancer microenvironment. Cell Biosci. 2023;13:217.
49. He Q, Lin Z, Wang Z, Huang W, Tian D, Liu M, Xia L. SIX4 promotes hepatocellular carcinoma metastasis through upregulating YAP1 and c-MET. Oncogene. 2020;39:7279–95.
50. Cohen-Dvashi H, Ben-Chetrit N, Russell R, Carvalho S, Lauriola M, Nisani S, Mancini M, Nataraj N, Kedmi M, Roth L, Köstler W, Zeisel A, Yitzhaky A, Zylberg J, Tarcic G, Eilam R, Wigelman Y, Will R, Lavi S, Porat Z, Wiemann S, Ricardo S, Schmitt F, Caldas C, Yarden Y. Navigator-3, a modulator of cell migration, may act as a suppressor of breast cancer progression. EMBO Mol Med. 2015;7:299–314.
51. Yao G, Yu S, Hou F, Xiao Z, Li G, Ji X, Wang J. Rab3B enhances the stabilization of DDX6 to promote lung adenocarcinoma aggressiveness. Mol Med (Cambridge, Mass). 2024;30:75.
52. Li M, Wang Z, Dong S, Xu Y. NAV3 is a novel prognostic biomarker affecting the immune status of the tumor microenvironment in colorectal cancer. J Immunol Res. 2022;2022:8337048.
53. Xu X, Gong C, Wang Y, Yin Z, Wang X, Hu Y, Fang Z. Bioinformatics analysis and experimental validation identified HMGA2/microRNA-200c-3p/LSAMP/Wnt axis as an immunological factor of patients with colorectal cancer. Am J Cancer Res. 2023;13:3898–920.
54. Kottorou A, Dimitrakopoulos FI, Diamantopoulou G, Kalofonou F, Stavropoulos M, Thomopoulos K, Makatsoris T, Koutras A, Kalofonos H. Small extracellular vesicles (sEVs) biogenesis molecular players are associated with clinical outcome of colorectal cancer patients. Cancers. 2023. https://doi.org/10.3390/cancers15061685.
55. Sun X, Hu F, Hou Z, Chen Q, Lan J, Luo X, Wang G, Hu J, Cao Z. SIX4 activates Akt and promotes tumor angiogenesis. Exp Cell Res. 2019;383:111495.
56. Li G, Hu F, Luo X, Hu J, Feng Y. SIX4 promotes metastasis via activation of the PI3K-AKT pathway in colorectal cancer. PeerJ. 2017;5: e3394.
57. Fellows RC, Chun SK, Larson N, Fortin BM, Mahieu AL, Song WA, Seldin MM, Pannunzio NR, Masri S. Disruption of the intestinal clock drives dysbiosis and impaired barrier function in colorectal cancer. Sci Adv. 2024;10:eado1458.
58. Chun SK, Fortin BM, Fellows RC, Habowski AN, Verlande A, Song WA, Mahieu AL, Lefebvre A, Sterrenberg JN, Velez LM, Digman MA, Edwards RA, Pannunzio NR, Seldin MM, Waterman ML, Masri S. Disruption of the circadian clock drives Apc loss of heterozygosity to accelerate colorectal cancer. Sci Adv. 2022;8:eabo2389.